2D Free-Standing Janus Gold Nanocrystal Superlattices

Qianqian Shi [1,2], Daniel E. Gómez [3], Dashen Dong [1,2], Debabrata Sikdar[4,5], Runfang Fu[1,2], Yiyi Liu[1,2], Yumeng Zhao[1,2], Detlef-M. Smilgies[6], and Wenlong Cheng [1,2]*

[1]Department of Chemical Engineering, Faculty of Engineering, Monash University, Clayton 3800, Victoria, Australia.

[2]The Melbourne Centre for Nanofabrication, 151 Wellington Road, Clayton 3168, Victoria, Australia.

[3]RMIT University, Melbourne, VIC, 3000, Australia

[4]Imperial College London, MSRH, W12 0BZ, UK

[5]Department of Electronics and Electrical Engineering, Indian Institute of Technology Guwahati, Guwahati, India 781039.

[5]Cornell High Energy Synchrotron Source (CHESS), Ithaca NY 14853, USA

* Address correspondence to wenlong.cheng@monash.edu

Keywords: plasmonic, self-assembly, free-standing, Janus, superlattice

Two-dimensional (2D) free-standing nanocrystal superlattices represent a new class of advanced metamaterials in that they can integrate mechanical flexibility with novel optical, electrical, plasmonic, and magnetic properties into one multifunctional system. The free-standing 2D superlattices reported to date are typically constructed from symmetrical constituent building blocks, which have identical structural and functional properties on both sides. Here, we report a general ligand symmetry-breaking strategy to grow 2D Janus gold nanocrystal superlattice sheet with nanocube morphology on one side yet with nanostars on the opposite side. Such asymmetric metallic structures lead to distinct wetting and optical properties as well as surface-enhanced Raman scattering (SERS) effects. In particular, the SERS enhancement of the nanocube side is about 20-fold of that of the nanostar side, likely due to a combined "hot spot + lightening rod" effects. This is nearly 700-fold of SERS enhancement as compared with the symmetric nanocube superlattices without Janus structures.

Janus nanostructures, which possess asymmetric shape and/or surface properties on their opposite sides, have attracted significant attention because of their novel applications in interface stabilizers[1], switchable devices[2], optical sensors[3], and catalysis[4]. In contrast to homogeneous or symmetric nanoarchitectures, the broken symmetry combines different properties from two incompatible sides, thus gives rise to anisotropic nature in a single system. Nevertheless, it is not trivial to fabricate structurally well-defined two-dimensional (2D) Janus nanoassemblies despite of numerous Janus particles synthesized in bulk solutions.

Recently, 2D frees-standing nanocrystal superlattices have been successfully fabricated, which exhibited unique mechanical[5], ion permeable[6], and plasmonic properties[7]. However, their constituent building blocks are typically symmetrical with identical material properties exhibited on both sides. It is interesting to find that surface chemistry does influence properties of 2D membranes/sheets. In the nanoparticle membrane reported recently[8], it was found that

a small difference (~6Å) in average ligand thickness between two sides could substantially change mechanical response to electron beams, as well as influence the SERS properties. Similar effects of asymmetric surface functionalities on properties of 2D films were also found for other materials systems[9]. In contrast, it is rarely reported that Janus nanocrystal building blocks could be used to assemble free-standing superlattices with excellent control over orientations of Janus building blocks due to complex temporal and spatial interaction forces during the assembly process. It is encouraging that the high-quality Janus quantum dot-gold heterodimers[10], and Janus Fe_3O_4-Au heterodimers [11], have been successfully used to fabricate superlattices. Nevertheless, it is difficult to assembly free-standing 2D nanoassemblies from Janus building blocks with perfect orientation and may be also challenging to extend it to non-spherical building blocks. Asymmetric metal deposition can be a practical way to obtain Janus metallic films, however, this method has been usually limited to micrometre-sized particles[12].

Here, we report a simple yet efficient two-step surface symmetry breaking approach (Figure 1a) to grow 2D Janus gold nanocrystal superlattices with well-defined dual surface morphology: one side with nanocube (NC) and the opposite side with nanostars. The as-obtained asymmetric 2D superlattices displayed distinct morphology-dependent surface wettability, optical properties, and SERR effects on opposite sides. We observed 20-fold higher SERS enhancement for NC side than that for nanostar side, which may be a result of the combination of the "lightning-rod effect" of star tips and "hot spot effects" originating from strong plasmonic coupling between NC building blocks.

Au NC building blocks were synthesized by the seed-mediated method[7a], which were then functionalized by thiolated PS ligands by the ligand exchange method. By the two-step drying-mediated self-assembly on a sessile droplet[5b], we could form a 2D close-packed Au NC superlattices (Figure 1b). To fabricate 2D Janus superlattice, PS ligands was selectively

removed by UV-ozone cleaning in a gentle and time-controlled manner so that gold surfaces of nanocrystals were partially exposed (Figure 1c). Such exposed area then served as nucleation/growth points for gold spikes growth through a surfactant-free chemical approach[13]. Cross-sectional scanning electron microscopy (SEM) images (Figure 1b-d) demonstrate the shape evolution from a symmetric NC monolayer to an asymmetric Janus structure with the star-like shape on top of NCs. This was further proved from the top-view SEM images (Figure 1e-f). To further visualise morphologies of individual Janus gold nanocrystals, we dissolved the Janus superlattices into chloroform using strong sonication. A high-resolution transmission electron microscopy (TEM) image (Figure 1g) clearly shows Janus nanoparticles with nanostars on one side of nanocubes.

According to the literature, the growth of spiky star-shaped structures starts with the deposition of Ag^0/AgCl on the nuclei, followed by the anisotropic growth of Au spikes in a gentle reduction process[14]. Therefore, numbers of ways can be used to finely control nanostar growth via controlling the exposed area of Au, Ag^+ concentration, and the concentration of gold precursor (Figures S1-6). Additionally, our methodology to fabricate Janus superlattices is general and robust: other types of building blocks including nanobipyramids (NBP), nanorods (NR) and nanospheres (NS), and vertical aligned NBP can be used as seeds to grow Janus nanostars as well (Figures S7-8).

The aforementioned Janus superlattices could stabilize as monolith in a free-standing manner, contributed from the residual ligands at the NC side and spiky nanostars that entangled with each other. To demonstrate this, a layer of poly (methyl methacrylate) was used as a sacrificial layer to release the monolayered Janus superlattice from the substrate in acetone. The maintenance of structural integrity was proved at three different magnifications. At the macroscopic scale, the Janus superlattice remains intact in the solvent as shown in Figure 2a; at the microscopic scale, such free-standing structure can still be maintained after transferring

to a holey Cu grid (Figure 2b); at the nanoscale, the TEM image clearly demonstrates a monolayered superlattice with entangled spikes (Figure 2c) which help maintain the mechanical robustness of the Janus superlattice. In contrast, the NC superlattice without the growth of spikes broke into small pieces after releasing into the acetone (Figure S9). Although partial removal of the ligands didn't destroy structural integrity of a free-standing superlattice at a dry state due to the residual PS ligands[15], chemical engtanglement of polystyrene ligands didn't provide sufficient stability. In contrast, entangled spikes could maintain structural integrity in acetone. Therefore, we concluded that entangled spikes are an important factor, which provided strong physical forces preventing from fragmentation in solvents.

We further characterized free-standing Janus superlattices using synchrotron-based small-angle x-ray scattering (SAXS). Both Janus and Au NC superlattices show well-defined scattering rings (insert images in Figure 2d and e). Corresponding one-dimensional SAXS patterns of both Au NC and Janus superlattice (Figure 2d and e) exhibit at least 5 distinguishable Bragg peaks with a lattice constant of 52 nm, which is consistent with the interparticle spacing of 52.8 ± 3.9 nm as obtained from the TEM image of the Janus superlattice (Figure S10). Those results indicate that the growth of nanostar didn't destroy the overall structural integrity of the 2D superlattices.

2D Janus gold nanocrystal superlattices exhibit distinct wetting and optical properties on opposite sides. The Janus wetting property is attributed to the asymmetric ligand distribution in our Janus superlattice. As shown in Figure 3a, the removal of PS on the top side of Au NC superlattice results in a more hydrophilic surface, further growth of stars on the ligand-free NC surface increases the contact angle (Figure 3b), from 50.3^{o} to 64.1^{o}. The contact angle of the opposite side of the Janus film is 96.1^{o} (Figure 3c), because of the hydrophobic PS ligands. Since the star side is ligand free, we believe the wettability can be further adjusted by additional functionalization of the star surface to meet different surface requirements in target applications.

We further investigated the optical properties of the Janus superlattice (Figure S11), and found that the Janus superlattice shows different reflectance and scattering properties on opposite sides, while exhibiting similar extinction properties. The plasmon modes of the stars are very complex, since they are highly dependent on morphology such as spike number, size, orientation, the symmetry of the nanoparticle[16]. Therefore, it is a very challenging task and out of our capabilities to make a detailed simulation on these Janus superlattices, instead, we analysed the optical properties and explain the properties-geometry relationship from the view of morphology dependence.

One of the most outstanding observations made with reference to our results, is the fact that the star-side exhibits significantly less light scattering than the NC-side (Figure 3d). This can be explained by considering the geometrical cross-section of the star-side films: closely-spaced sharp grooves face up the incident field and these grooves increase slowly in diameter as they approach the surface of the nanocubes. In this configuration, it is possible to excite gap plasmon modes[17], which are modes that propagate toward the bottom of the grooves (toward the metal nanocube). Depending on the curvature variation of the grooves, it is possible to achieve the regime of adiabatic nano-focusing of light[18] which results in almost complete absorption of energy, and hence to a suppression of scattering. In our structures, it is likely that the interaction of light with the star-side of the Janus films results in the excitation of a distribution of these gap plasmon modes, some of which can in principle lead to adiabatic nano-focusing of light. The distribution of sizes and orientations of the nano-grooves in our samples precludes the excitation of a coherent excitation across the surface of the Janus film, leading to some parasitic scattering.

For the reflection peaks, the reflectivity of NC-side is lower than that of the star-side (Figure 3e), which was ~ 52.9% in the range of 650-950 nm. The lower reflectance indicates that the NC-side possesses anti-reflective properties and is able to reduce the loss of light absorption,

resulting in a better light trapping property. When it comes to the extinction spectra under transmission mode (Figure 3f), both Star-to-NC side and NC-to-Star side show similar spectra, which possess a slightly red-shifted peak around 550 nm (origins from the Au NC) and an additional shoulder at the near-infrared region (results from spikes) in comparison to the original Au NC superlattice. These results indicate that our approach to fabricate Janus structure provides an effective way to rationally design and control surface properties.

It is well-known that star-shaped gold nanoparticles have so-called "lightning rod effect' due to the intense electromagnetic field that generated at their tips[13], which makes them excellent candidates for SERS substrates[19]. Using 4-ATP as the probe molecule, we performed the SERS measurement on both star and NC side of Janus superlattices (Figure 4a-b). Two prominent peaks at 1078 and 1582 cm^{-1} are observed from the SERS spectra at different laser wavelengths (Figure 4c-f). These two modes are assigned to the *a*1-type vibration modes of ν(C-S) and ν(C-C), which have been ascribed to the electromagnetic (EM) effect that arises from the enhancement of the electric field at the metal surface[13].

We used the ν(C-S) vibration at 1078 cm^{-1} to compare the SERS enhancement of different samples and summarize the results in Figure 4g. Both the star and NC side show better SERS enhancement in comparison to the original Au NC superlattice. Also, the SERS intensity shows a strong excitation wavelength dependence, which may be attributed to the electromagnetic (EM) enhancement mechanism. It is known that the SERS enhancement factor is proportional to the fourth power of the EM field. The highest SERS enhancement is normally observed when excitation laser wavelength matches closely to the plasmonic resonance band, at which the EM field is the strongest [7a, 20]. At a laser wavelength of 514 nm, which is close to the plasmonic resonance peak of Au NCs, the coupling between Au NCs dominates the EM effect, thus resulting in a comparable enhancement for star-side and NC-side. With the laser wavelength closer to the resonance peak of the star (over 900 nm in our system), the effect

from star arises due to their sharp tips ("lightning-rod effect") and finally result in the increased intensity of $a1$ vibration modes. This enlarges the difference from the opposite sides and finally result in a Janus SERS performance. At laser wavelengths of 633, 782 and 830nm, the NC-side always generates the highest signal. In particular, the enhancement of the SERS efficiency on the NC-side is around 20-fold as compared to the star-side (for both laser 782 and 830 nm), and is nearly 700 (at laser 782 nm) and 440-fold (at laser 830 nm) in comparison with the Au NC superlattice. Notably, this high enhancement arises despite the similar number density and interparticle spacing of nanoparticles, thus can be only attributed to the structural difference. As evidenced in Figure S12, the NC-side possesses not only close-packed NC nanoparticles but also spiky structures underneath after ligand removal. Such a unique structure may integrate "lightning-rod effect" and plasmonic coupling between NC nanoparticles, thus resulting in a "collective" EM enhancement effect. Our results here highlight the effect of the combination of two properties into one Janus system for enhanced optical sensitivity as compared to a symmetrical one.

Our work successfully demonstrated a Janus superlattice with distinct morphology, surface wettability, optical properties, and SERS performance on opposite faces. The Janus superlattice also features a free-standing ability due to the entangled spiky structure, and has the ability to maintain the lattice structure from the original Au NC superlattice. Furthermore, we found the Janus structure could integrate the properties from two sides, and finally boosts the overall SERS efficiency of the superlattice. Our work therefore opens up the possibility of a new superlattice design rule through breaking the morphology symmetry and provides an effective approach to strengthen the material properties by integration of different properties into one structure. This novel Janus structure can also provide a platform and model for the design of 2D superlattices with multiple functionalities for potential applications in optical, biological and chemical sensors, and optical energy devices.

Supporting Information

Supporting Information is available from the Wiley Online Library or from the author.

Acknowledgements

The authors thank financial support from Australian Research Council via Discovery Grant scheme DP170102208 and FT140100514. D.S. acknowledges the support of a H2020-MSCA individual fellowship. This work was performed in part at the Melbourne Centre for Nanofabrication (MCN) in the Victorian Node of the Australian National Fabrication Facility (ANFF). The authors also gratefully acknowledge the use of facilities at the Monash Centre for Electron Microscopy. They also thank the staff of the SAXS/WAXS beamline at the Australian Synchrotron, Victoria, Australia. CHESS is supported by NSF award DMR-1332208. The authors thank Dr. Ranwen Ou for water contact angle measurement. They also thank Dr. Lim Wei Yap for helping with the Table of Contents image drawing.

Competing financial interests

The authors declare no competing financial interests.

Figures

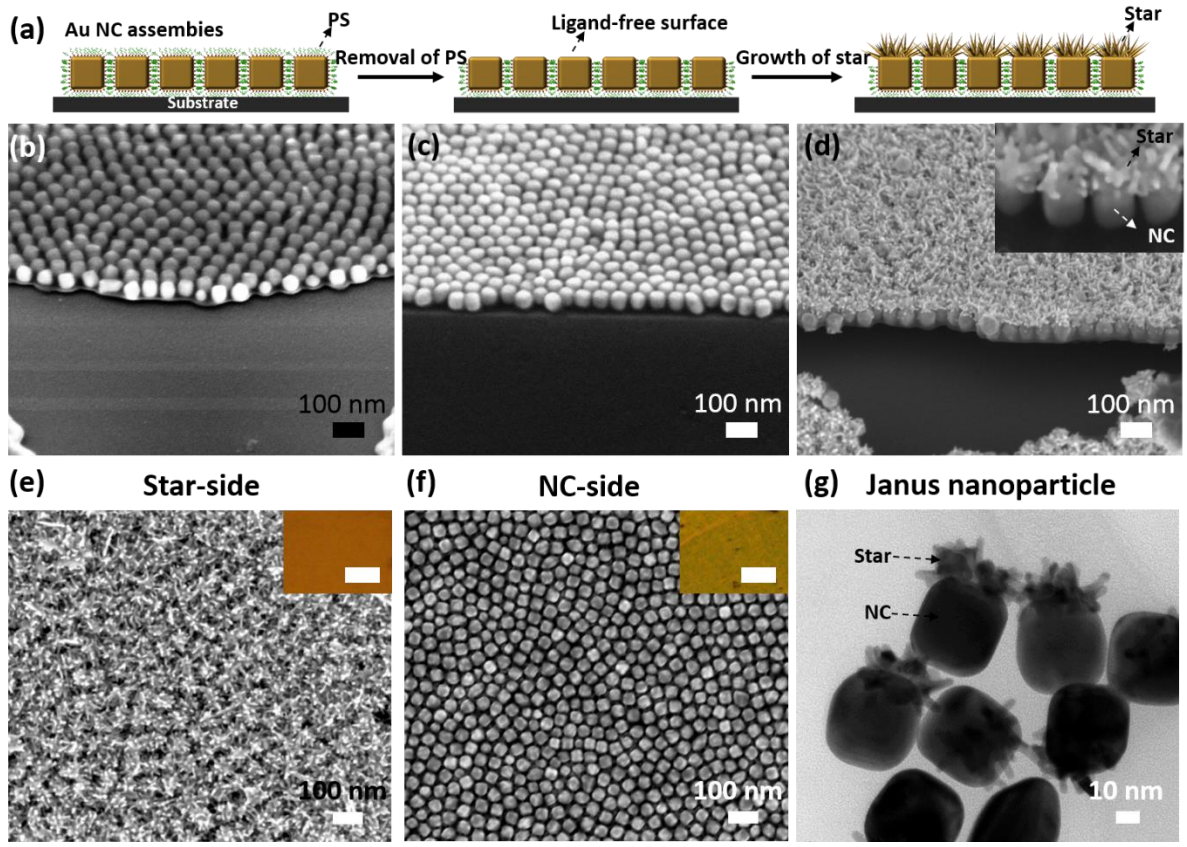

Figure 1. Fabrication of the Janus superlattice. (a) Schematic of the fabrication of 2D Janus superlattice. The morphology evolution of NC superlattice change from (b) the original symmetry NC superlattice, to (c) top side ligand-free NC superlattice, and finally (d) Janus NC superlattice according to SEM images at a tilted (52^{o}) view. SEM images of the distinct sides with (e) star-shape and (f) NC shape, scale bars in inserts represent 10 μm. (g) TEM image of individual Janus nanoparticles. Inserts in (e and f) represent optical images of corresponding superlattices under a reflection mode.

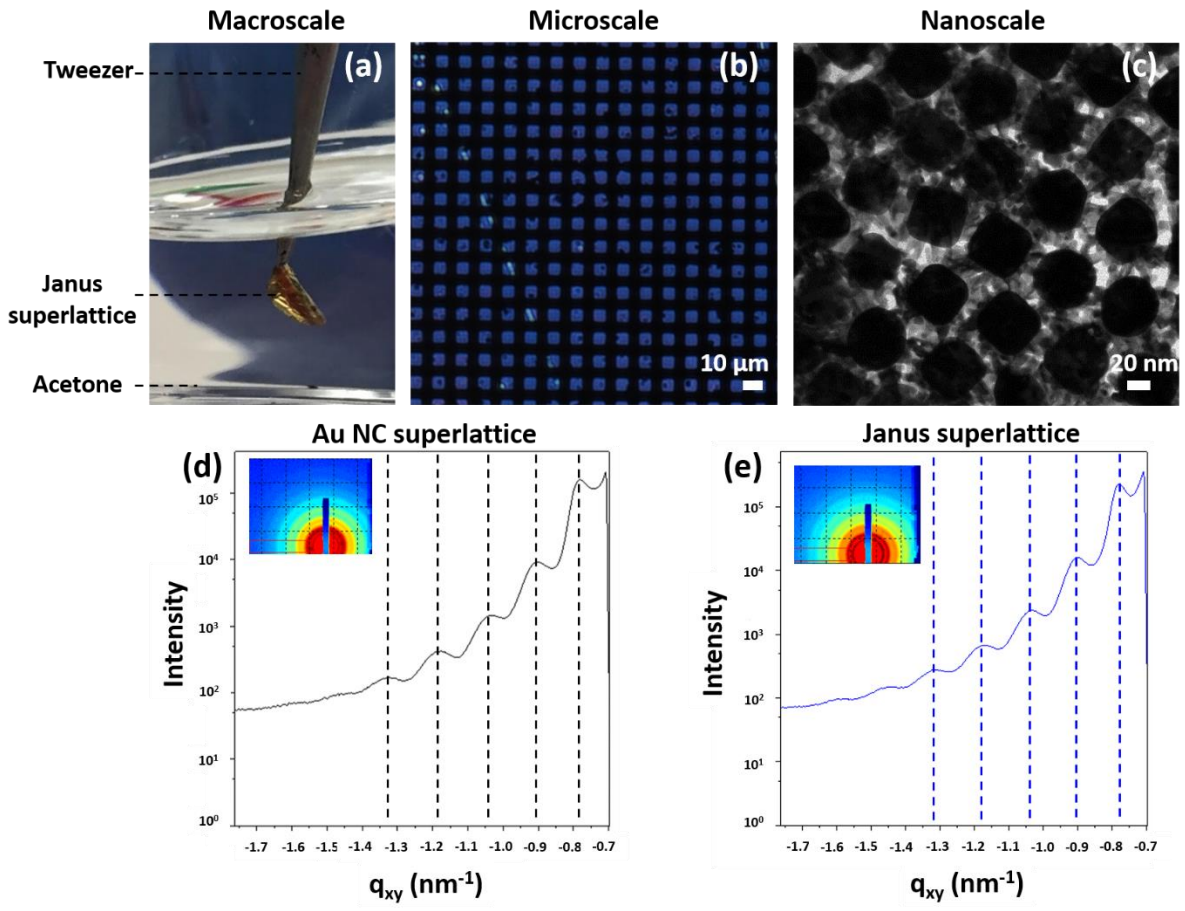

Figure 2. Maintenance of structural integrity of the free-standing Janus superlattice. Characterization of free-standing 2D Janus superlattice at the (a) macro-, (b) micro-, and (c) nanoscale. SAXS 2D (inserts) and 1D patterns of (d) Au NC and (e) Janus superlattice. The 1D patterns were integrated from the inserts of 2D images without removal of form factor, showing at least 5 Bragg peaks.

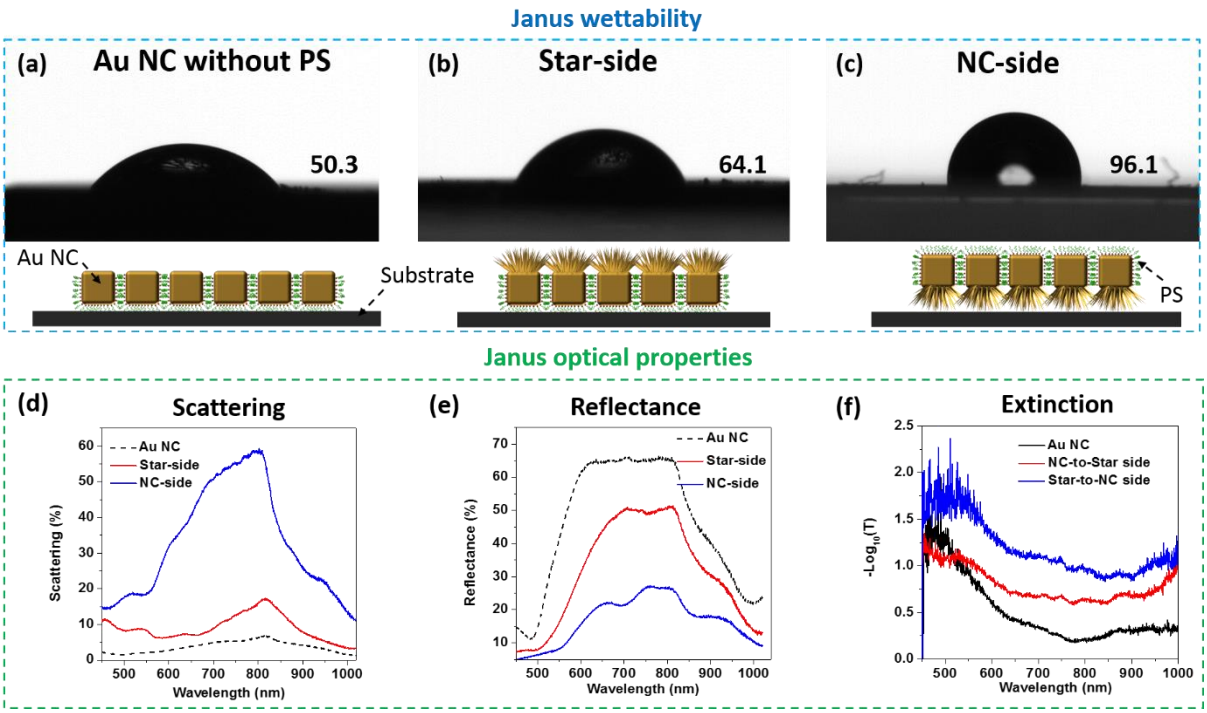

Figure 3. Janus wettability and optical properties. Contact angle measurement of (a) surface ligand-free Au NC, (b) star-side and (c) NC-side of the Janus superlattice. The schematic diagram highlights the morphology differences of samples in (a-c). (d) Scattering, (e) reflectance, and (f) extinction properties from opposite sides of Janus superlattice in comparison to the original Au NC superlattice.

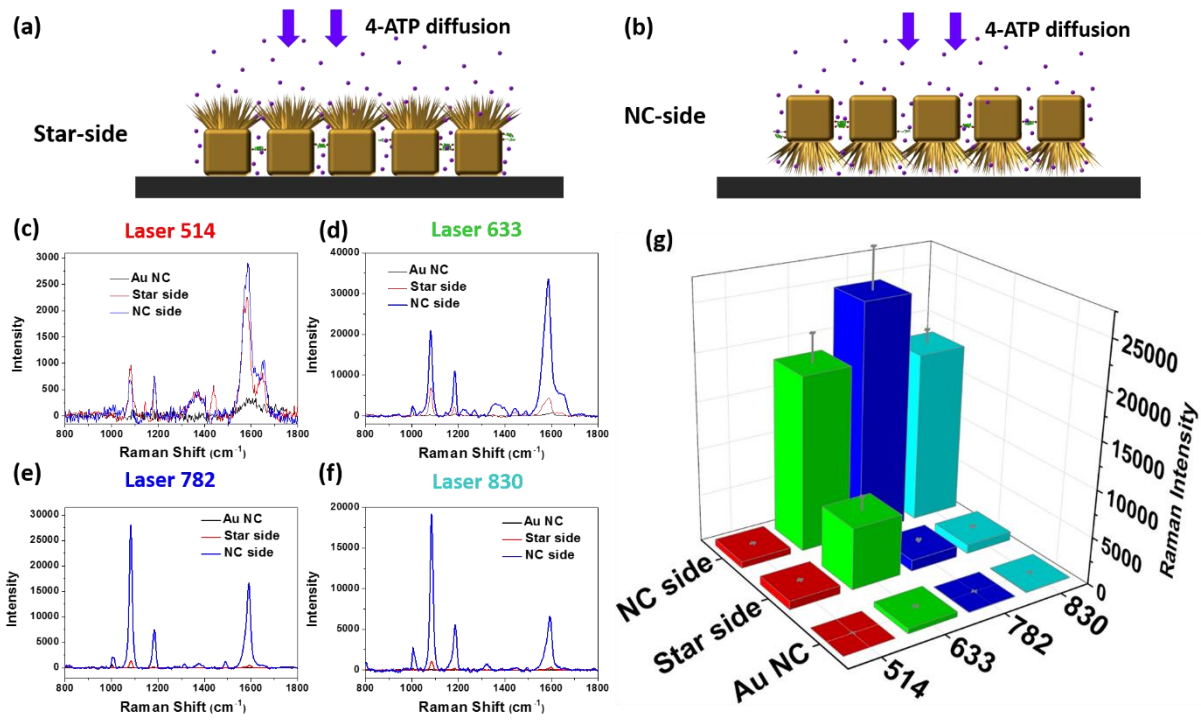

Figure 4. Application of the 2D Janus superlattice as a SERS substrate. Schematic of the measurement of SERS performance on (a) star-side and (b) NC side. SERS spectra of 4-ATP vapour from the Janus superlattice and original NC superlattice with laser wavelengths of (c) 514 nm, (d) 633 nm, (e) 782 nm, and (f) 830 nm. (g) Summary of corresponding SERS intensities of the above samples at the vibrational band of 1078 cm^{-1}.

Reference

[1] a) F. Liang, K. Shen, X. Qu, C. Zhang, Q. Wang, J. Li, J. Liu, Z. Yang, *Angew. Chem., Int. Ed.* **2011**, *50*, 2379; b) A. Walther, M. Hoffmann, A. H. E. Müller, *Angew. Chem., Int. Ed.* **2008**, *47*, 711.

[2] Z. Yu, C.-F. Wang, L. Ling, L. Chen, S. Chen, *Angew. Chem., Int. Ed.* **2012**, *51*, 2375.

[3] a) Y. Zhao, H. Gu, Z. Xie, H. C. Shum, B. Wang, Z. Gu, *J. Am. Chem. Soc.* **2013**, *135*, 54; b) T. Nisisako, T. Torii, T. Takahashi, Y. Takizawa, *Adv. Mater.* **2006**, *18*, 1152.

[4] a) B. Jurado-Sánchez, S. Sattayasamitsathit, W. Gao, L. Santos, Y. Fedorak, V. V. Singh, J. Orozco, M. Galarnyk, J. Wang, *Small* **2015**, *11*, 499; b) S. Crossley, J. Faria, M. Shen, D. E. Resasco, *Science* **2010**, *327*, 68.

[5] a) K. E. Mueggenburg, X.-M. Lin, R. H. Goldsmith, H. M. Jaeger, *Nat. Mater.* **2007**, *6*, 656; b) K. J. Si, D. Sikdar, Y. Chen, F. Eftekhari, Z. Xu, Y. Tang, W. Xiong, P. Guo, S. Zhang, Y. Lu, Q. Bao, W. Zhu, M. Premaratne, W. Cheng, *ACS Nano* **2014**, *8*, 11086; c) W. Cheng, M. J. Campolongo, J. J. Cha, S. J. Tan, C. C. Umbach, D. A. Muller, D. Luo, *Nat. Mater.* **2009**, *8*, 519.

[6] S. Rao, K. J. Si, L. W. Yap, Y. Xiang, W. Cheng, *ACS Nano* **2015**, *9*, 11218.

[7] a) Q. Shi, K. J. Si, D. Sikdar, L. W. Yap, M. Premaratne, W. Cheng, *ACS Nano* **2016**, *10*, 967; b) Q. Shi, D. Sikdar, R. Fu, K. J. Si, D. Dong, Y. Liu, M. Premaratne, W. Cheng, *Adv. Mater.* **2018**, *30*, 1801118; c) A. Tao, P. Sinsermsuksakul, P. Yang, *Nat. Nanotechnol.* **2007**, *2*, 435.

[8] Z. Jiang, J. He, S. A. Deshmukh, P. Kanjanaboos, G. Kamath, Y. Wang, S. K. R. S. Sankaranarayanan, J. Wang, H. M. Jaeger, X.-M. Lin, *Nat. Mater.* **2015**, *14*, 912.

[9] a) Z. Zheng, C. T. Nottbohm, A. Turchanin, H. Muzik, A. Beyer, M. Heilemann, M. Sauer, A. Gölzhäuser, *Angew. Chem., Int. Ed.* **2010**, *49*, 8493; b) Y. Liu, F. Liang, Q.

Wang, X. Qu, Z. Yang, *Chem. Commun.* **2015**, *51*, 3562; c) L. Zhang, J. Yu, M. Yang, Q. Xie, H. Peng, Z. Liu, *Nat. Commun.* **2013**, *4*, 1443.

[10] H. Zhu, Z. Fan, Y. Yuan, M. A. Wilson, K. Hills-Kimball, Z. Wei, J. He, R. Li, M. Grünwald, O. Chen, *Nano Lett.* **2018**, *18*, 5049.

[11] D. Jishkariani, Y. Wu, D. Wang, Y. Liu, A. van Blaaderen, C. B. Murray, *ACS Nano* **2017**, *11*, 7958.

[12] a) Y. M. Sabri, A. E. Kandjani, S. J. Ippolito, S. K. Bhargava, *Sci. Rep.* **2016**, *6*, 24625; b) V. N. Paunov, O. J. Cayre, *Adv. Mater.* **2004**, *16*, 788; c) J. Du, R. K. O'Reilly, *Chem. Soc. Rev.* **2011**, *40*, 2402; d) A. Perro, S. Reculusa, S. Ravaine, E. Bourgeat-Lami, E. Duguet, *J. Mater. Chem.* **2005**, *15*, 3745; e) A. Walther, A. H. E. Müller, *Chem. Rev.* **2013**, *113*, 5194.

[13] K. J. Si, D. Sikdar, L. W. Yap, J. K. K. Foo, P. Guo, Q. Shi, M. Premaratne, W. Cheng, *Adv. Opt. Mater.* **2015**, *3*, 1710.

[14] a) L.-C. Cheng, J.-H. Huang, H. M. Chen, T.-C. Lai, K.-Y. Yang, R.-S. Liu, M. Hsiao, C.-H. Chen, L.-J. Her, D. P. Tsai, *J. Mater. Chem.* **2012**, *22*, 2244; b) Y. Hsiangkuo, G. K. Christopher, H. Hanjun, M. W. Christy, A. G. Gerald, V.-D. Tuan, *Nanotechnol.* **2012**, *23*, 075102.

[15] K. J. Si, P. Guo, Q. Shi, W. Cheng, *Anal. Chem.* **2015**, *87*, 5263.

[16] L. Shao, A. S. Susha, L. S. Cheung, T. K. Sau, A. L. Rogach, J. Wang, *Langmuir* **2012**, *28*, 8979.

[17] C. Ng, L. W. Yap, A. Roberts, W. Cheng, D. E. Gómez, *Adv. Funct. Mater.* **2017**, *27*, 1604080.

[18] T. Søndergaard, S. M. Novikov, T. Holmgaard, R. L. Eriksen, J. Beermann, Z. Han, K. Pedersen, S. I. Bozhevolnyi, *Nat. Commun.* **2012**, *3*, 969.

[19] a) J. Fang, S. Du, S. Lebedkin, Z. Li, R. Kruk, M. Kappes, H. Hahn, *Nano Lett.* **2010**, *10*, 5006; b) S. Park, J. Lee, H. Ko, *ACS Appl. Mater. Interfaces* **2017**, *9*, 44088; c) A. Shiohara, J. Langer, L. Polavarapu, L. M. Liz-Marzán, *Nanoscale* **2014**, *6*, 9817.

[20] a) Y. Chen, K. J. Si, D. Sikdar, Y. Tang, M. Premaratne, W. Cheng, *Adv. Opt. Mater.* **2015**, *3*, 919; b) R. A. Álvarez-Puebla, *J. Phys. Chem. Lett.* **2012**, *3*, 857; c) J. Ye, J. A. Hutchison, H. Uji-i, J. Hofkens, L. Lagae, G. Maes, G. Borghs, P. Van Dorpe, *Nanoscale* **2012**, *4*, 1606; d) A. D. McFarland, M. A. Young, J. A. Dieringer, R. P. Van Duyne, *J. Phys. Chem. B* **2005**, *109*, 11279.

A general ligand symmetry-breaking strategy is introduced to design and fabricate two-dimensional (2D) Janus gold nanocrystal superlattice sheet with nanocube on one side yet with nanostars on the opposite side. Such asymmetric structure displays distinct morphology-dependent surface wettability, optical properties, and SERS effects on opposite sides, providing a novel way to design and tune the material properties of 2D superlattices.

Keywords: plasmonic nanocrystal, self-assembly, free-standing, Janus, superlattice

Qianqian Shi [1,2], Daniel E. Gómez [3], Dashen Dong [1,2], Debabrata Sikdar[4], Runfang Fu[1,2], Yiyi Liu[1,2], Yumeng Zhao[1,2], Detlef-M. Smilgies[5], and Wenlong Cheng [1,2*]

Title: 2D Free-Standing Janus Gold Nanocrystal Superlattices